JOURNAL OF GEOPHYSICAL RESEARCH, VOL. 94, NO. A5, PAGES 5367-5381, MAY 1, 1989

Ground-Based Imaging of Detached Arcs, Ripples in the Diffuse Aurora, and Patches of 6300-Å Emission

MICHAEL MENDILLO AND JEFFREY BAUMGARDNER

Center for Space Physics, Boston University, Boston, Massachusetts

JAMES PROVIDAKES

School of Electrical Engineering, Cornell University, Ithaca, New York

A period of coordinated, multidiagnostic observations of the subauroral ionosphere conducted in April 1985 resulted in a series of optical and plasma characterizations of three distinct phenomena: arcs detached from the diffuse aurora, undulations in the equatorward edge of the diffuse aurora, and isolated patches of emission in the *F* region trough. The optical features were observed by the 6300-Å imaging system in Boston University's Mobile Ionospheric Observatory located at the Millstone Hill observatory; plasma observations were made by the Millstone incoherent scatter radar, Air Force Geophysics Laboratory satellite radio beacon polarimeters, and the Defense Meteorological Satellite Program (DMSP) energetic particle detectors. The detached arc observations showed that strong *F* region enhancements occured in both 6300-Å emission and total plasma content, suggesting an electron precipitation source essentially similar to the plasma sheet population that causes the diffuse aurora and the poleward wall of the *F* region trough. The rippled features along the equatorward edge of the diffuse aurora were associated with strong electric fields and large radial ion temperature gradients, topics discussed in detail in a companion paper. The isolated and long-lived patches of 6300-A emission have no corresponding *F* region plasma enhancements, but are associated with enhanced radar returns from the *E* region. Nearly simultaneous DMSP observations point to the importance of ion precipitation effects as a cause for these *F* region optical and *E* region plasma enhancements. The entire set of observations (detached arc, ripples, and patches) show that ground-based imaging and radio techniques can provide detailed spatial and temporal coverage of phenomena hitherto observed by satellite only

1. INTRODUCTION

1.1. *Background*

Satellite-borne (ISIS) imaging systems at 3914 Å and 5577 Å have observed cases of arcs detached from the auroral oval [*Anger et al.*, 1978]. Additional ISIS observations have shown patches of emission at the same wavelengths, also equatorward of the diffuse aurora [*Moshupi et al.*, 1977]. Using photographs from a Defense Meteorological Satellite Program (DMSP) satellite, *Lui et al.* [1982] have described a series of large-scale undulations or ripples in the equatorward edge of the diffuse aurora in observations recorded in the visible/IR band. The Dynamics Explorer imaging system has recorded cases of mid-latitude stable auroral red (SAR) arcs at 6300 Å, in some cases showing a patchy structure along the arc [*Craven et al.*, 1982]. Further interpretations of the ISIS data on detached arcs and patches have been made by *Wallis et al.* [1979], while *Kelley* [1986] has discussed ionospheric instabilities resulting from intense sheared flow as a possible cause for the ripples in the diffuse aurora. The SAR arc observations from DE have been examined in comparison to standard [*Rees and Roble*, 1975] models by *Kozyra et al.* [1982].

Paper number 88JA04245.
0148-0227/89/88JA-04245$05.00

In the present study, we report on observations when all three phenomena (patches, ripples, detached arcs) occurred during a single period of very high geomagnetic activity (April 20–22, 1985). The optical observations were made at 6300 Å from a mid-latitude site normally considered to be subauroral. Simultaneous observations made by incoherent scatter radar, satellite-borne in situ probes, and satellite radio beacon techniques provided plasma parameters at selected locations within the imager's field of view. These measurements represent the first coordinated observations of such events from the ground and thus offer opportunities to examine the manifestations of strong magnetospheric processes imposed upon the subauroral ionospheric *F* region using a higher spatial and temporal coverage than is normally available from satellite based studies.

1.2. *The April 1985 Clustered Diagnostics Campaign*

Boston University's Mobile Ionospheric Observatory (MIO) contains a monochromatic, low-light-level imaging system that has been developed for a variety of geophysical and astronomical applications [*Baumgardner and Karandanis*, 1982]. During the moon-down period in April 1985, the MIO operated from a site near the Millstone Hill Incoherent Scatter Radar Observatory as part of the ground-based observing network established for the Active Magnetospheric Particle Tracer Explorers (AMPTE) chemical release exper-

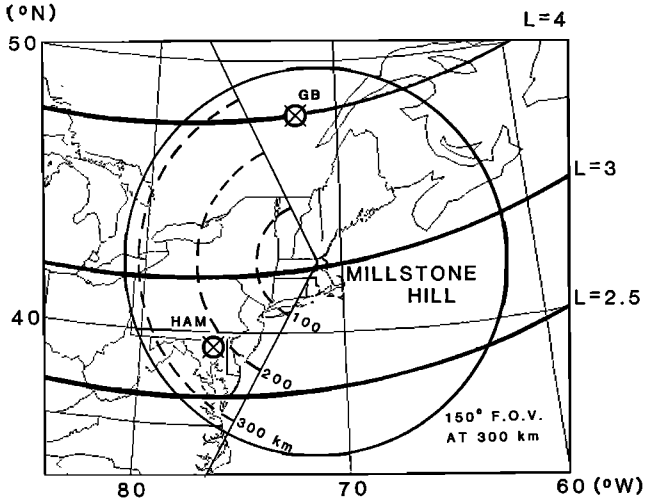

Fig. 1. Map of the field of view (FOV) for imaging observations from Millstone Hill (42.6°N, 71.5°W) using zenith angles <75° and assuming a 6300-A mean emission height of 300 km. The Millstone Hill radar operated using azimuth scans from 210° to 340° at an elevation of 20°. The altitudes of 100, 200, and 300 km within this sector are indicated. Ionospheric intersection points are also shown for 300-km altitudes along ray paths to the GOES satellite from stations at Goose Bay (Labrador) and Hamilton (Massachusetts). These satellite radio beacon observations yield total electron content data.

iments in the geomagnetic tail. During the period April 20–22, a period of very high geomagnetic activity, no AMPTE releases were performed, and thus the MIO imaging system was operated in wide-angle mode during several periods to study large-scale *F* region disturbances. Coordinated measurements using the Millstone Hill radar and several satellites were conducted by *Providakes et al.* [this issue] in a detailed study of dynamical processes associated with the trough/diffuse aurora region. In this paper we concentrate on the optical features in considerably more detail.

When operating in "all-sky" mode, the imager's field of view (FOV) actually records emission down to zenith distances of only 75° due to trees and buildings near the horizon. For observations at 6300 Å, the projection of this FOV to a mean emission height of 300-km is given in Figure 1. The optical images spanning this region are "unwarped" and mapped to the 300-km-plane and viewed from above in order to facilitate comparisons with other observing techniques (see *Mendillo et al.* [1987] for details of this approach). The choice of 300 km as the height to portray the optical data represents an average altitude for the various excitation emission processes that yield 6300-Å photons. The $O(^1D)$ state can be produced by normal *F* region chemical recombination (airglow), from excitation by hot ambient electrons (SAR arcs), or by several energetic particle precipitation mechanisms (diffuse aurora, auroral arcs). In each case, excitations below 200 km experience severe quenching (deactivation via collisions) during the 147-s lifetime of the $O(^1D)$ state. Thus, long-lived emissions at 6300 Å are rightly assigned to the F region. Heights of 250–350 km are typical for diffuse aurora and airglow [*Mendillo et al.*, 1987], while 200 km is more appropriate for auroral arcs [*Rees and Roble*, 1986], and 400 km for SAR arcs [*Rees and Roble*, 1975]. When two or more features are evident in the same image, the assumption of a single emission height could lead to minor differences between the positions assigned to optical patterns and those of related plasma processes observed by radar or satellites. Such correlation problems become severe only at very low elevation angles, regions not treated in this report.

Figure 2 contains a summary of the geomagnetic indices that characterize the April 19–22, 1985, period. As can be seen, the geomagnetic storm that began on April 19, 1985, developed into one of the strongest disturbances of the recent solar minimum period. With Kp = 7–8 and Dst = 120–150(γ) at the peak of the main phase (early on April 21), auroral morphologies rarely seen at mid-latitudes appeared throughout the MIO's field of view. The intervals of optical observations are indicated on the bottom of Figure 2, and in Plate 1 we present samples of the three types of optical features that were recorded during these periods. These observations were made using a 6300-Å filter that has a 12 Å wide full width at half power (FWHP) with integration times of 30 s. In Plate 1*a*, a well-formed arc detached from the diffuse aurora is observed at 2100 LT; in Plate 1*b* (2148 LT) the arc is no longer present, and the diffuse aurora displays large structured patterns; Plate 1*c* (taken 40 min later) shows the diffuse aurora shifted to the north with undulations still quite noticeable; Plate 1*d* shows examples of the isolated patches of 6300-Å emission that were observed from 2000 to 2300 LT on the following night.

In the section below, we describe in more detail the time histories of the three optical features shown in Plate 1. In section 3 we present simultaneous plasma measurements, and

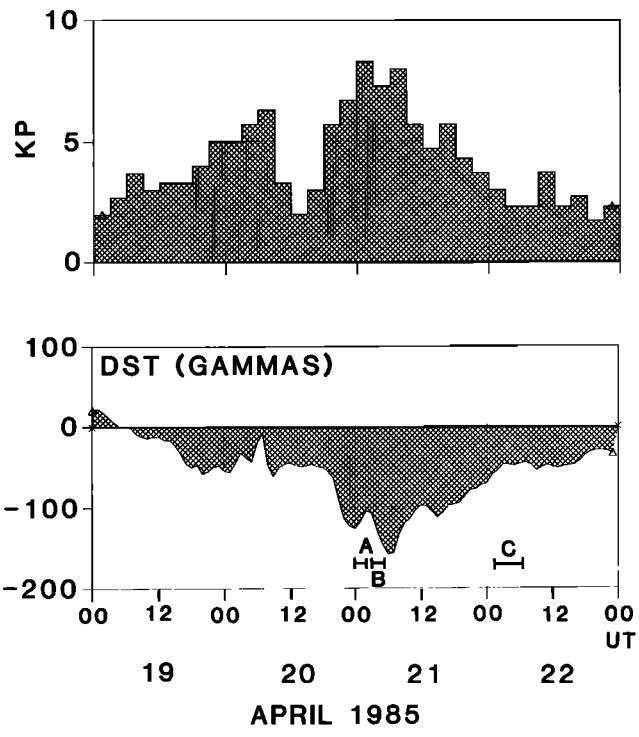

Fig. 2. Geomagnetic indices for the period April 19–22, 1985. Periods of optical observations from Millstone Hill are indicated: (A) a detached arc, (B) ripples in the diffuse aurora, and (C) patches of emission.

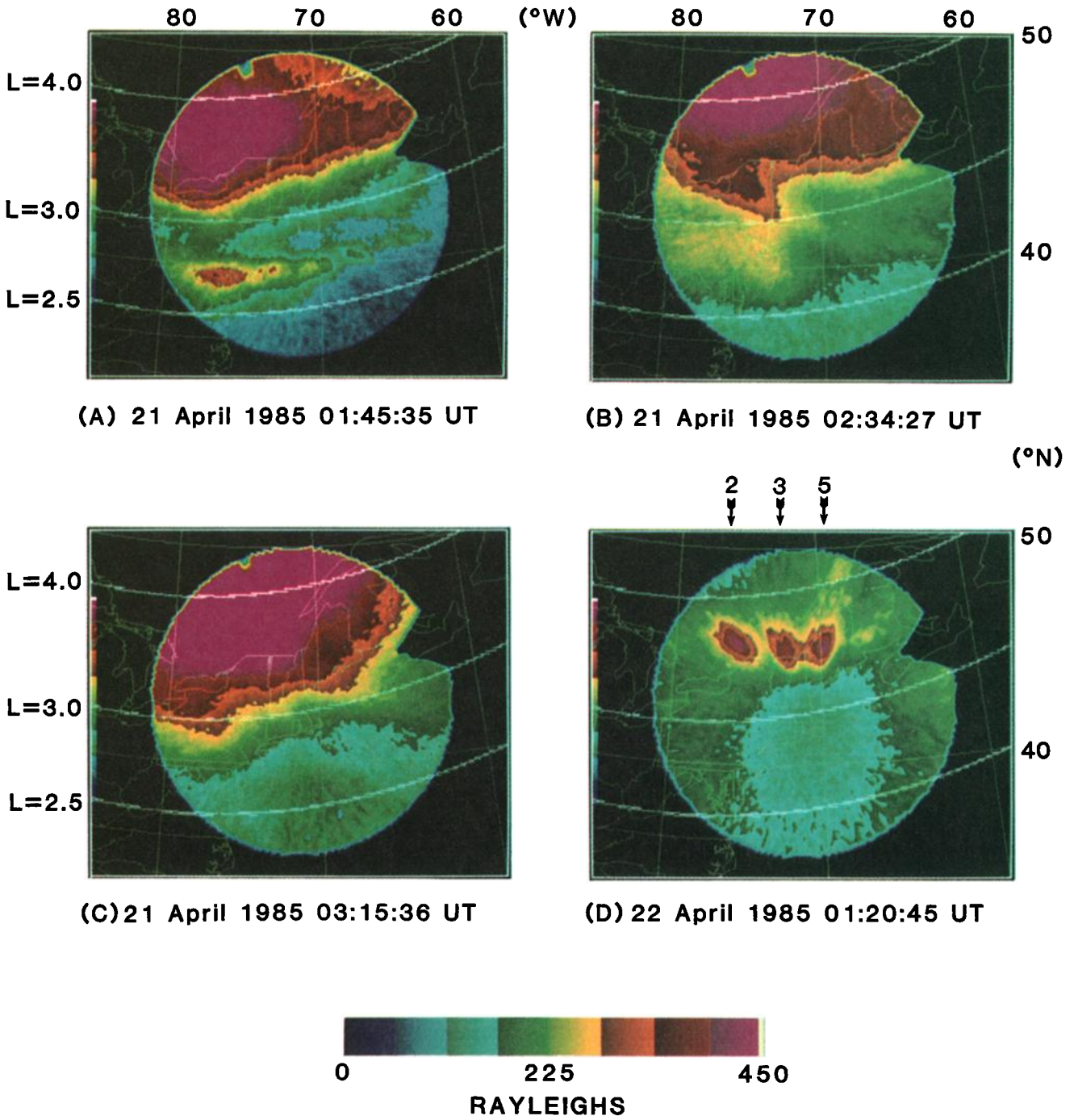

Plate 1. Examples of four structures in 6300-A images taken on April 21 and 22, 1985, from a site near the Millstone Hill observatory. The dark triangular feature in each image is a building that obscures a portion of the all-sky FOV in the northeast. The four panels exhibit (*a*) a detached arc, (*b*) large ripples in the diffuse aurora, (*c*) small ripples in the diffuse aurora, and (*d*) patches of emission. Times are given in UT; for the Millstone Hill meridian, LT = UT − 4:45. Geographic latitudes and longitudes are given together with geomagnetic *L* shells.

in section 4 we discuss mechanisms responsible for the coupled effects.

2. Optical Observations

2.1. *Detached Arc Characteristics*

The detached arc shown in Plate 1*a* occurs at L=2.7 during the peak phase in geomagnetic activity (as defined by *Kp* in Figure 2). The arc is brighter at earlier (westward) points, with a > 200-km-latitude thickness at 75° W; there is some evidence for small-scale structure ($\leq$ 50 km) near and within the arc. While the lack of emission east of the observing meridian is unambiguous, the intensity falloff at the western edge of the FOV may be due to lens vignetting effects. There is evidence for a tenuous connection to the diffuse aurora a few degrees poleward of the arc. The intensities in the arc are comparable to those seen in the diffuse aurora. Several of these features agree with those reported by *Anger et al.* [1978] for the ISIS events: occurrence in local time, L shell alignment, latitudinal width when the arc is diffuse, and connection to the diffuse aurora. The ISIS events, however, were at much higher L shells (typically L=6–7), occurred during the recovery phases of storms, and were attributed to E region altitudes due to the strong appearance of the features in 5577 Å and 3914 Å. It should be noted in this context that visible aurora was observed south of the Millstone zenith during this period, but no images in 5577 Å were taken. As shown in Plate 1, the detached arc lasted for less than an hour after the first image was acquired, another consistency with the Anger et al. estimates for lifetimes.

To summarize, the morphology of the detached arc of April 21, 1985, appears to conform in every major way with the only extensive analysis previously conducted for detached arcs [*Anger et al.*, 1977]. This event extends the observational data base to mid-latitudes, using ground-based 6300-Å observations arising from F region altitudes.

2.2. *Characteristics of Ripples in the Diffuse Aurora*

In the detached arc image (Plate 1*a*), there is also a hint of ripples along the equatorward edge of the diffuse aurora. During the next 50 min the diffuse aurora surged equatorward by nearly 1/2 L, and thus it is uncertain if the detached arc faded or moved beyond the imager's FOV. For the next hour, the FOV was dominated by a remarkable series of rippled structure in 6300-Å emission. In Plate 1*b*, a single large undulation bends noticeably toward later local times (eastward); it has a crest-to-trough spatial amplitude of 150 km, corresponding to 1/3 L value. With no other crest in the FOV, the equivalent wavelength of the pattern exceeds 1000 km or more. In Plate 1*c*, an image taken 41 min later, the diffuse aurora is at approximately the same location, but now the undulations have smaller crest-to-trough spatial amplitudes (30–60 km) spanning 0.1–0.2 L; there is also evidence for multiple cycles along the diffuse aurora boundary with crests separated by 300 km.

The characteristics summarized above are consistent with those found in the DMSP images described by *Lui et al.* [1982]. The ground-based and satellite observations are in agreement for the undulation forms, spatial amplitudes and wavelengths, occurrence patterns in local time, associated magnetic activity levels, and overall duration. The 6300 Å observations once again place the phenomena in the F region, thus affording opportunities to investigate sources using high-resolution ground-based optical and radio techniques.

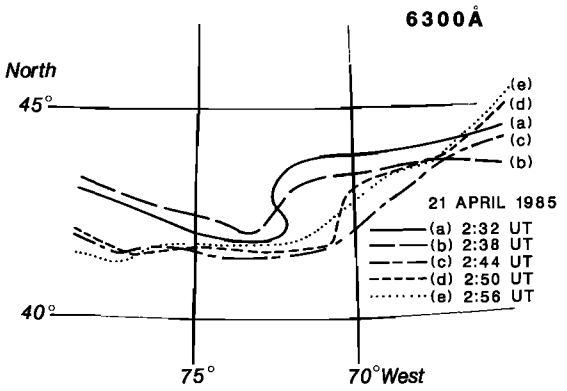

Fig. 3. Evolution of large ripples on the equatorward edge of the diffuse aurora with a 6-minute time resolution from 0232 to 02:56 UT on April 21, 1985. The isophote boundary plotted is for the 280-R level (approximately the boundary between the yellow and orange coding in Plate 1).

In the *Lui et al.* [1982] study, the DMSP images captured rippled patterns over much larger regions than are accessible to single-site ground-based systems. Time resolution was limited, however, by the 90-min satellite orbit. The present set of observations can be used to see if the undulations propagate along the auroral boundary or change amplitudes in place. Figure 3 compares time histories for undulation patterns early in the evening when long wavelengths and large crest-to-trough amplitudes occurred. The impression from these 6-min observations, as well as from other episodes later in the evening, is that the features are essentially fixed in location and vary only in amplitude as time progresses.

The April 1985 observations showing ripples in the diffuse aurora prompted a search of other MIO data-taking periods at Millstone Hill for indications of similar effects. In Plate 2, four images taken on April 27, 1984, display features not seen during the April 1985 period. On this night, the 6300-Å images recorded mid-latitude airglow toward the southern horizon, an east-west airglow depletion through the zenith that results from the F region trough, a narrow, faint SAR arc imbedded in the trough, and diffuse aurora to the north. After 0700 UT (0214 LT), the diffuse aurora intensified, small undulations appeared along the equatorward edge, and the entire auroral pattern rotated away from L shell alignment. The undulations in Plate 2 are comparable to the smallest cases seen in Plate 1 and Figure 3. They occur during the early morning hours, in contrast to all of the cases described by *Lui et al.* [1982] and *Kelley* [1986] when only late afternoon/evening cases were found.

Magnetic activity for this period is summarized in Figure 4. As seen from Figures 4*a* and 4*b*, the *Kp* and *Dst* indices show that the images on April 27 were taken during the recovery phase of a large geomagnetic storm that lasted for more than 3 days. In Figure 4*c*, high time resolution auroral electrojet indices for the April 27 period show typical substorm surges that last for an hour or more (e.g., near 0300 and 0700 UT) The appearance of diffuse aurora and SAR

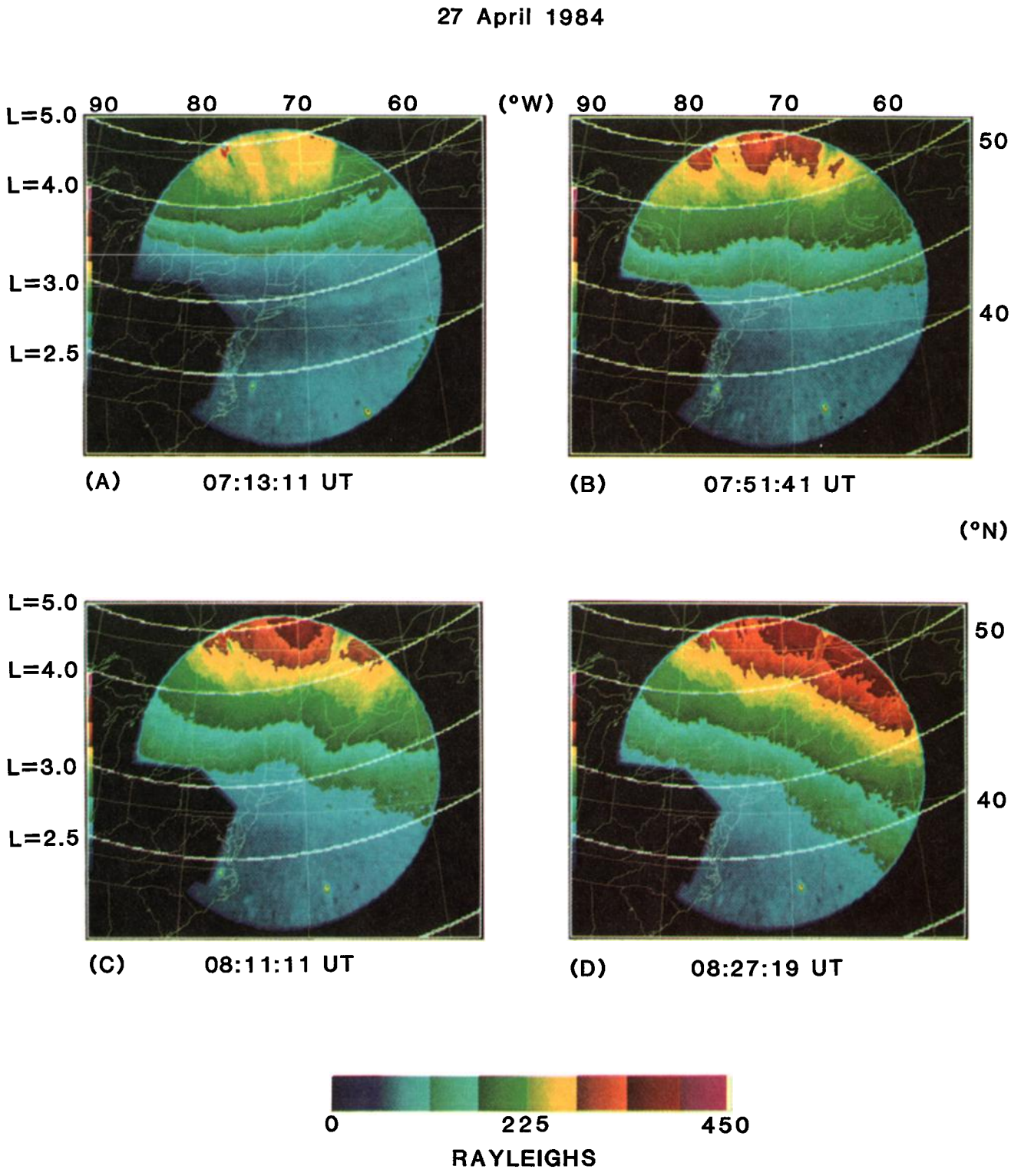

Plate 2. 6300-Å images taken on April 27, 1984, at a site near Millstone Hill. The dark wedge-shaped feature is a building obscuring a full view to the southeast. (*a*) A faint SAR arc embedded in the *F* region trough is visible crossing the zenith from east to west, with a somewhat brighter diffuse aurora to the north, (*b*) An intensification and equatorward movement of the diffuse aurora with some structuring along the equatorward edge, (*c*) Well-formed undulations along the diffuse aurora and a slight tilt to later local times (*d*) A strong diffuse aurora, with reduced undulation, tilted significantly from quiet *L* shell alignment. In all frames, the SAR arc remains weak, but visible, moving to lower latitudes as time progresses. The two bright spots toward the southern edge of the FOV are emissions from Jupiter and Saturn.

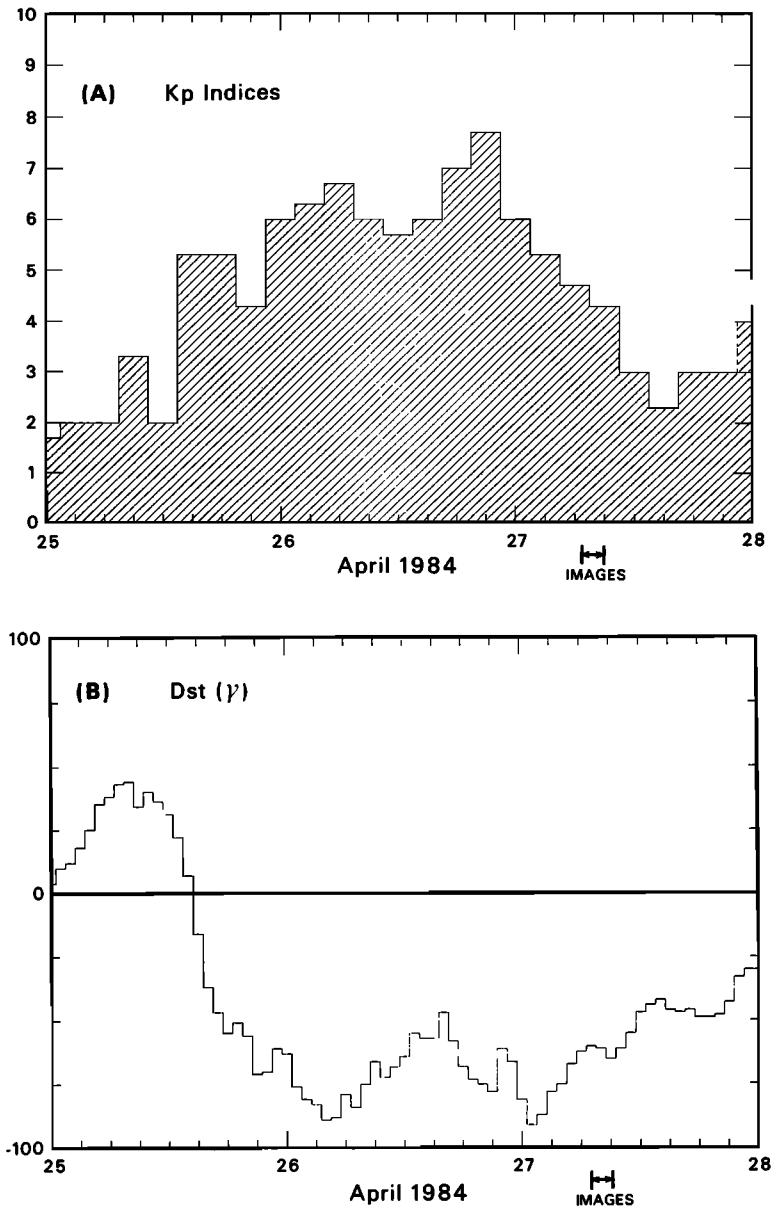

Fig. 4 Geomagnetic activity indices for April 25–27, 1984, with the times of optical observations given in Plate 2 noted. In (*a*) and (*b*), three-hour *Kp* and hourly *Dst* data are used to characterize the overall geomagnetic storm levels that occurred during the 3-day period. In (*c*) high time resolution auroral electrojet indices are shown for the period of optical data presented in Plate 2.

arc at $L < 4$ are consistent with these conditions. Notice, however, that the dramatic shift of the diffuse aurora away from L shell alignment occurred at the time of the very large but temporally brief surge in the AE index. The strong confinement of the electrojet disturbance to the AL component points to an impulsive westward current in the early morning hours.

2.3. *Characteristics of Patches*

Plate 1*d* gives an example of the 6300-Å patches of emission that occurred for several hours on the night of April 22, 1985. The sizes of the patches varied during the course of the observing period but were always a few hundreds of kilometers in diameter. The somewhat oval appearance and alignment toward the observing site suggest that the features were extended in altitude and thus did not present a thin emission layer to the fish-eye lens system. In Plate 3, examples of patches are given during the course of the evening. It is clear that they are long-lived, wax and wane in size and brightness, occasionally merge or divide, and drift slowly to the west (at 50–100 m/s) and to lower L shells. Figure 5 summarizes the time histories of the entire set of patch observations. As can be seen from the time code (with 15 min resolution), the patch locations at any given time are very nearly L shell aligned, with movements to lower L values throughout the premidnight period. The slow westward drift implies that the source region moves to later local times at a speed nearly equal to the corotation speed. The patch structures summarized in Figure 5 seem to disappear as they

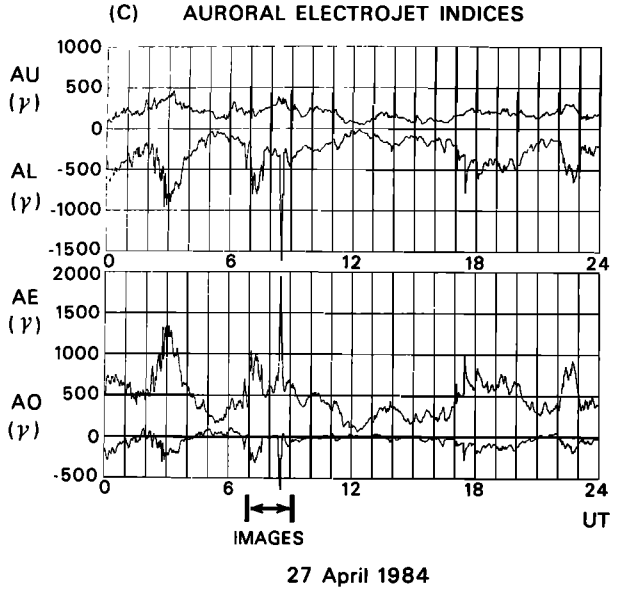

Fig. 4. (continued)

approach the edge of the imager's FOV. As described earlier, lens effects (vignetting) always reduce apparent brightness levels far from the zenith, and thus we do not suggest that the patches actually vanished when they approached the $L \simeq 3.2$–3.4 region near 77°W. Indeed, simultaneous measurements made by Battelle's MASP (mobile automatic scanning photometer) systems located in Michigan, Montana, and Washington recorded patches of 5577-Å emission (attributed to the 150 to 200-km region) and patches of 6300-Å emission from the *F* region that resembled a structured SAR arc during the 2040–0700 UT period (D. Slater, private communication, 1987).

The patches of emission at 3914 Å and 5577 Å observed by the ISIS satellite system [*Moshupi et al.*, 1977] were attributed to the 100–km–altitude range. They occurred somewhat later (2100 LT) and at lower latitudes (L=4–4.5) than the detached arcs (1800 LT and L=6–7). In 6300-Å emission, the patches were weak (< 200 R) and appeared as slight enhancements in a broad region (~ 10° latitude) of 6300-Å emission (~ 300 R) extending equatorward from the boundary of the diffuse aurora. Simultaneous ISIS 2 Langmuir probe electron temperature and density data placed the patches in the vicinity of the plasmapause. One of the morphological differences between the April 1985 patches and the ISIS data set is the displacement of the patches from the diffuse aurora. *Moshupi et al.* [1977] found displacements ranging from 0.5° to 7° geographic, with most cases within a few degrees. For the April 1985 case, the diffuse aurora was never observed to be within the 5°–7° geographic latitude north of the patches' location in the imager's FOV.

3. Plasma Observations

During the April 20–21, 1985, period, several ground-based radio and satellite-borne in situ diagnostic systems observed plasma parameters close to or within the imager's FOV depicted in Figure 1. These included DMSP and HILAT electron and ion detectors, the Millstone Hill incoherent scatter radar, and satellite radio beacon observations. In relating 6300-Å emission and "simultaneous" plasma patterns, it must be recalled that the ~ 147 s lifetime of the $O(^1D)$ state introduces a small uncertainty in relating detailed time histories of optical and plasma observations. This could be serious if interest centered on small time scales (< 60 s) and/or if narrow-beam photometer measurements were made. Under such conditions, strong convection effects could, for example, separate plasma and optical signatures. For the present case, however, where all-sky images, 30-s integration times, and temporal patterns in the many minutes to hours domain are examined, we treat correlations between plasma and optical effects in the broad, morphological sense.

3.1. *Detached Arc Event*

The ionospheric storm that occurred in response to the high level of geomagnetic activity during the April 21–22 period has been described by *Mendillo et al.* [1987] using satellite radio beacon observations at the L=4 (Goose Bay) and L=2.7 (Hamilton) intersection points shown in Figure 1. As shown in Figure 6, the total electron content (TEC) observations made at L=2.7 revealed the "classic pattern" of large enhancements at dusk (2300–2400 UT), followed by a very rapid transition to low, troughlike TEC values [*Mendillo*, 1971, 1973]. Severe cases of this pattern have been treated in detail by *Mendillo et al.* [1974] with several events similar in intensity (Kp=8–9) to the April 1985 period. For such cases, the steep $d(\mathrm{TEC})/dt$ transition across the dusk meridian has been interpreted as due to the observing ray path moving from within the plasmasphere to beyond it. Subsequent observational and modeling studies have confirmed that enhanced magnetospheric convection imposed upon the *F* region can result in the predusk buildup in mid-latitude TEC and in its steep decline across a plasmapause contracted to $L < 3$ in the postsunset period [*Evans*, 1973; *Anderson*, 1976; *Tanaka and Hirao*, 1973].

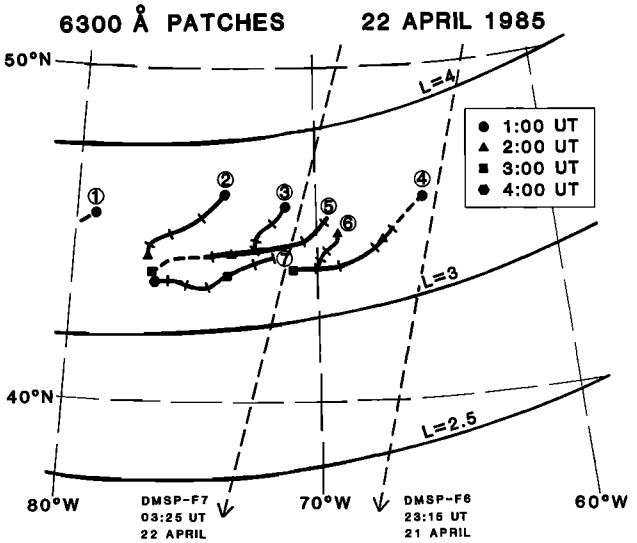

Fig. 5. Time history of all patches of 6300-Å emission recorded on the night of April 22, 1985. The individual patches are labeled for cross-reference to Plate 1 and Plate 3. Hourly symbols and quarter-hour tick marks give patch center locations throughout the observation period. Subsatellite trajectories of two DMSP passes over the region are indicated. The energetic particle data taken during these times are given in Figure 9.

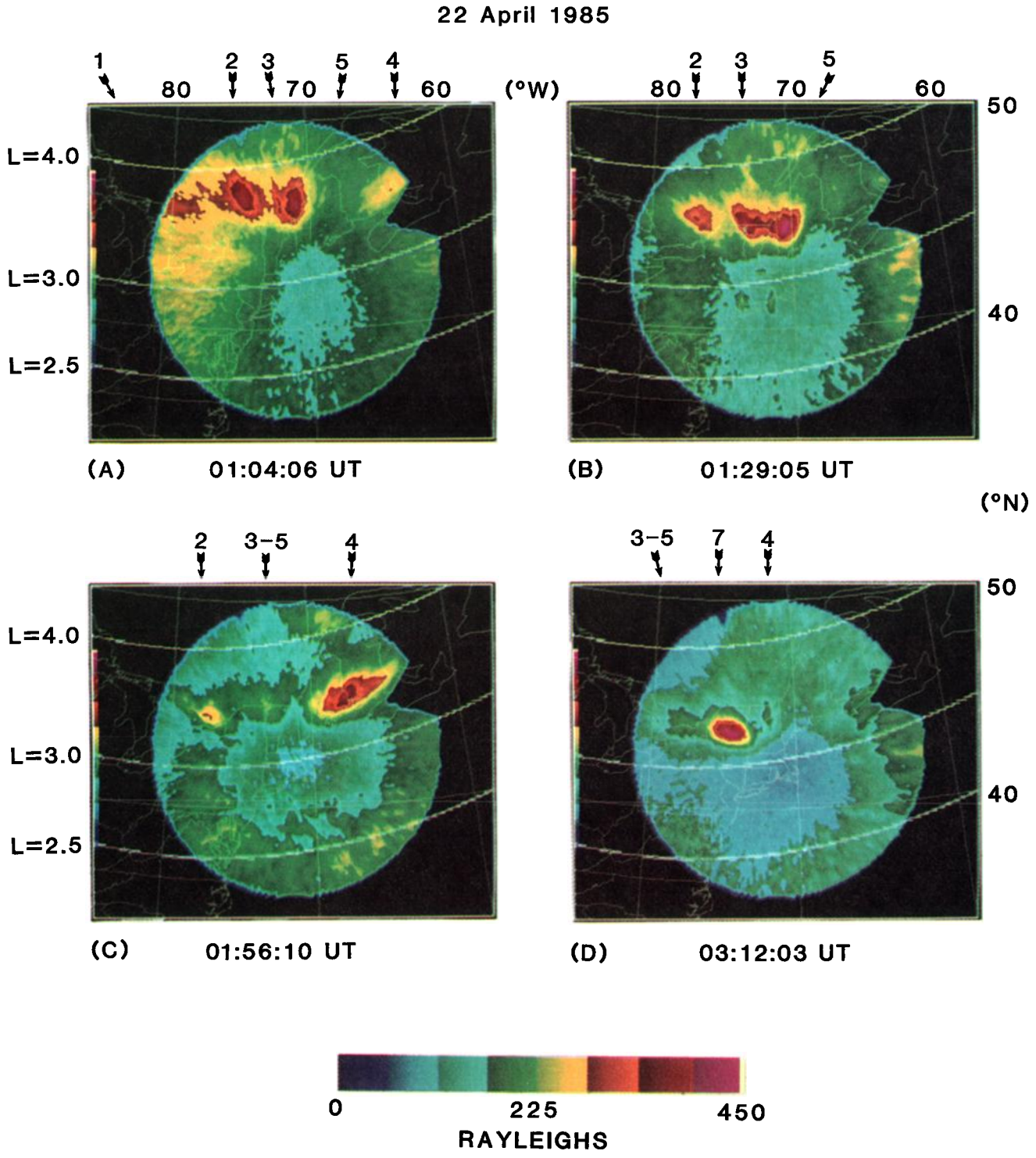

Plate 3. Examples of patches of 6300-Å emission recorded during the premidnight hours of April 22, 1985, from a site near the Millstone Hill observatory. The dark triangular feature is a building obscuring part of the northeast FOV. In each panel, the patches are numbered for reference to Plate 1 and Figure 5. Note that patches 2, 3, and 5 appear in Plate 1*d* at a time between those shown Plates 3*a* and 3*b*.

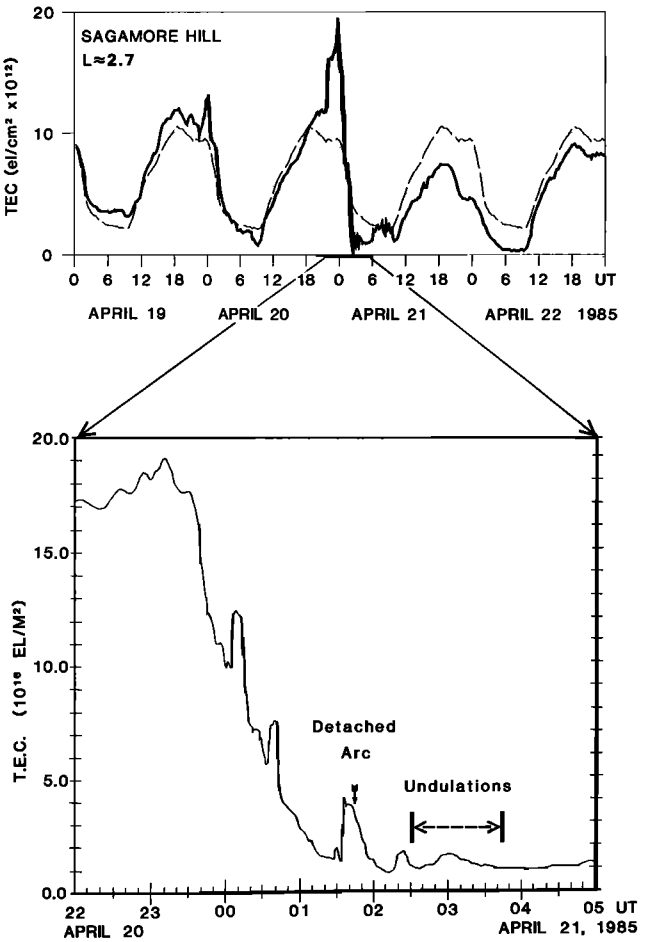

Fig. 6. (Top) Total electron content (TEC) observations during the period April 19–22, from the Hamilton-GOES ray path that intersects the 6300-A image at L=2.7 (see Figure 1). The solid curve gives 15-min TEC values showing a classic ionospheric storm in comparison to monthly median conditions (dashed curve). (Bottom) High-resolution TEC data for the time period encompassing the detached arc and undulations in the diffuse aurora near L=2.7.

In the bottom panel of Figure 6, we present new high time resolution TEC data for the L=2.7 site at 70° W that, as shown in Plate 1*a*, coincides with the detached arc location at 0145 UT. Note that in the period of rapid decline of TEC that signals the end of the initial (positive) phase of F region storm behavior, there are actually several reversals (TEC enhancements) that are not captured in the low resolution (15-min digitizations) given in the upper panel of Figure 6. As the TEC ray path passes into the trough, bursts of production occur that yield plasma enhancements of 2–4 x 10^{12} el/cm^2. These are substantial increases comparable in magnitude to the TEC enhancements associated with the diffuse aurora that form the poleward wall of the trough in TEC. While cloud cover prevented optical observations after 0400 UT, the TEC nighttime increases seen after 0600 UT are typical of F region enhancements associated with excursions of the diffuse aurora to mid-latitudes. As discussed in the following section, ion precipitation patterns may play a key role in both phenomena.

3.2. *Period of Structured Diffuse Aurora*

In a companion paper, *Providakes et al.* [this issue] have presented a comprehensive study of the ionospheric trough region observed during the full nighttime period of April 20 and the 0300–0400 UT period of April 21 using the Millstone radar, MIO images, and simultaneous DMSP and HILAT measurements. On the night of April 21, Providakes et al. present DMSP particle data at 0300 UT (their Figure 5) that show ion and electron precipitation onsets near L = 2.8–3.1, in agreement with the location of the diffuse aurora boundary in Plate 1*c* even though the DMSP satellite was over a location 3 hours earlier in local time. The particle data showed separations of the major boundaries in ion and electron fluxes, with the ion populations being ~0.6 L equatorward of the major electron precipitation. The suggestion that ion precipitation effects play important roles during auroral morphology excursions to mid-latitudes was further portrayed in DMSP data for April 20 when major ion populations were detected equatorward of the precipitating electron fluxes. A distinct zone of ion fluxes occurred 0.7 L equatorward of the major ion and electron boundaries (their Figure 12). The low-latitude ion boundary coincided with the foot of the poleward wall of the trough. As will be discussed in section 4, detached ion populations might also contribute to the detached arc pattern and the patches in 6300-Å emissions shown in Plate 1.

3.3. *Patches of 6300-Å Emission*

The "red patches" observed on April 22, 1985, represent perhaps the most interesting, and certainly the most elusive, of the entire MIO data set taken at Millstone Hill. A comparison of Figures 1 and 5 shows that the entire set of events fell between the satellite radio beacon monitoring points at L = 4 and L = 2.8. The TEC and scintillation activity at these points showed very low plasma contents, with minor small-scale irregularities [*Mendillo et al.* 1987]. As shown in Figure 6, April 22 was the second night (negative phase) of a severe ionospheric storm. The patches of emission thus occurred over a narrow latitude region within an F region electron density and TEC trough that spanned the entire FOV (L = 2.5 to 4).

The Millstone radar operated on April 22 in the so-called Cornell mode described by *Providakes et al.* [this issue], that is, with the antenna fixed at 20° elevation and scanning over the azimuth range 220°–340°. This observing scheme was developed to optimize measurements of line-of-sight drifts and trough density structures along the edge of the diffuse aurora. A comparison of Figures 1 and 5 shows that in confining the scans to westward directions, many of the patches eluded radar diagnostics at or near 300 km. Nevertheless, the radar did scan through at least one patch early in the evening and beneath several others later in the evening. The Millstone observations for April 22 were not treated by Providakes et al. because no diffuse aurora or trough poleward wall features were within the radar or imager fields of view. We will, therefore, describe them in some detail below.

Figure 7 contains a tracing of the 6300-Å isophote contours from Plates 3*a* and 3*d* superimposed upon the Millstone radar observing grid. In the left panel (0104 UT), as the radar crosses the onset of optical emission at azimuths 255°–260°, the radar signatures from the low-altitude range

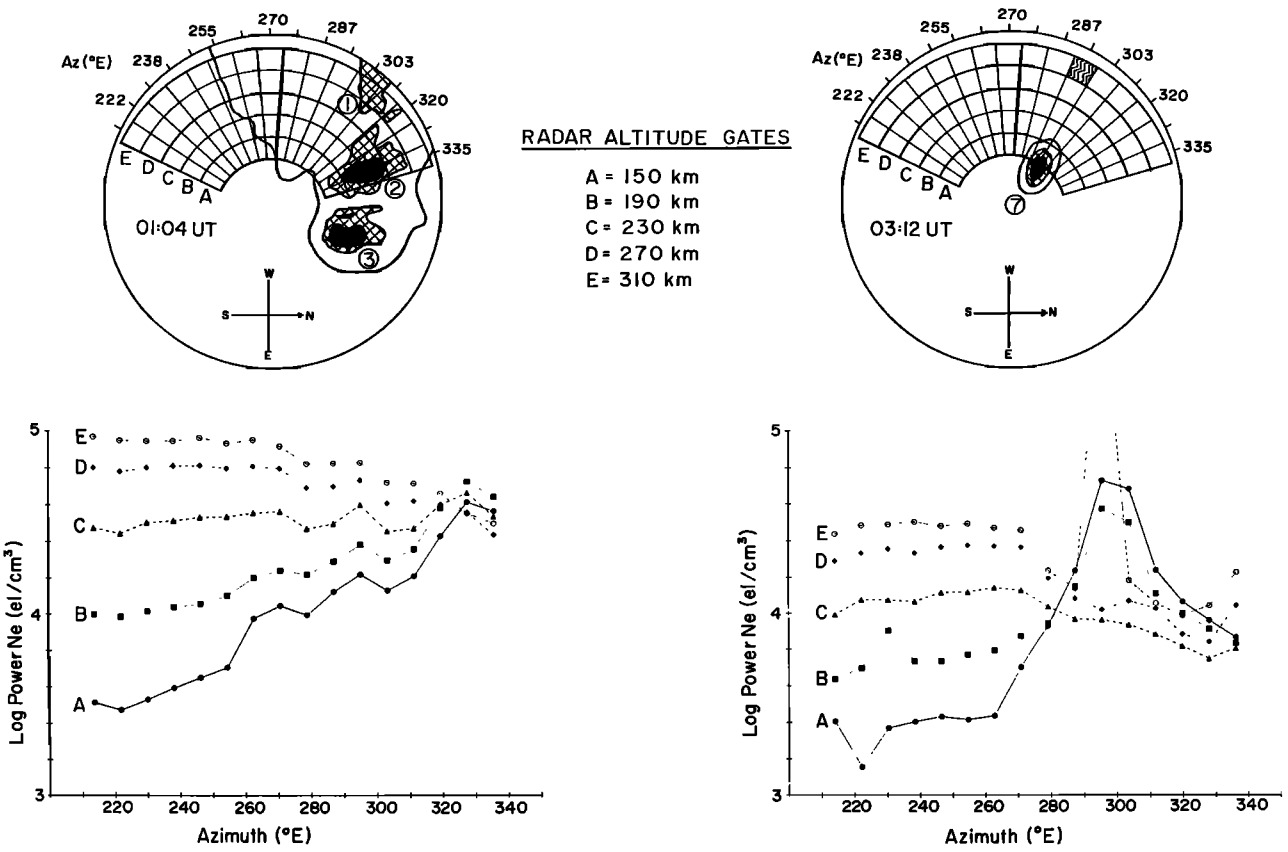

Fig. 7. Two cases of coincident imaging and radar scans through a region of 6300-Å patches. The "Cornell mode" radar azimuth scan at 20° elevation is portrayed with individual altitude gates ("pixels") indicated. The 6300-Å images are shown via tracings of the iosphote contour levels, with three domains indicated: brightest emission (solid shading), intermediate brightness (cross-hatched shading), and faintest level above background (outermost contour line). The Millstone radar returns are portrayed in "log (power)" equivalent electron density units to indicate that neither temperature nor composition changes are taken into account in the analysis scheme used to derive N_e from the observed power returns. For the 0312 UT case (upper right), the altitude gate where "anomalous echoes" were observed is indicated by zigzag hatching (see text for additional discussion).

gates A (150 km) and B (190 km) begin to show increased power returns. At azimuths 300°–310°, the radar crosses the bright patch 1 far to the west in Plate 1*a* and Figure 5. Altitude gates D (270 km) and E (310 km) show only a gentle decrease in *F* region returns with no evidence of plasma enhancements near the optical feature. At the lower-altitude gates, however, the power returns continue to increase, reaching maxima in the last azimuth points directly beneath patch 2. There are small enhancements at 230 km, larger ones at 190 km, and an order of magnitude effect at 150 km.

In the right panel of Figure 7, we present a second illustration, this time with the single bright patch 7 shown in Plate 3*d*. Over the low-azimuth (low-latitude) portion of the scan (215°–270°), the ionospheric profiles are typical of the trough region. As the radar scanned under the 6300-Å patch (azimuths 295°–303°), very large enhancements are seen in the lower-altitude gates A (150 km) and B (190 km). The densities above 200 km show decreases, as in the previous illustrations, except for the returns from the highest-altitude gate, E (310 km). The Millstone data for this particular return are well off scale and would have, under normal Millstone analysis rules, been discarded as a so-called "satellite echo." However, in a recent study of "anomalous echoes," *Foster et al.* [1988] argue that such cases are actually geophysical events and not coherent echoes from satellites or space debris, as had been thought. The spectra of these returns exhibit the characteristic features of field-aligned currents (FACs). We refer the reader to the Foster et al. study for a more thorough summary of this effect. For our purposes, we merely want to point out that the optical patches seen near the equatorward edge of the trough are associated with enhanced power returns from below 200 km, and that no *F* region power enhancements are seen except for the occasional "anomalous echoes" associated with FACs.

To document the altitude separation of the optical and radar events even more clearly, we present in Figure 8 two additional cases. In both panels, patch 7 is depicted at its assumed 300-km emission point, and the Millstone altitude gate with the largest power return is depicted with dots. For the optical feature to be at the latitude/longitude coincident with the radar signature, the optical features would have to be mapped using an emission height greater than the 300 km employed here. If the optical features were assigned to 150–190 km, they would be mapped to sites closer to the radar/MIO site and thus be even more separated from the

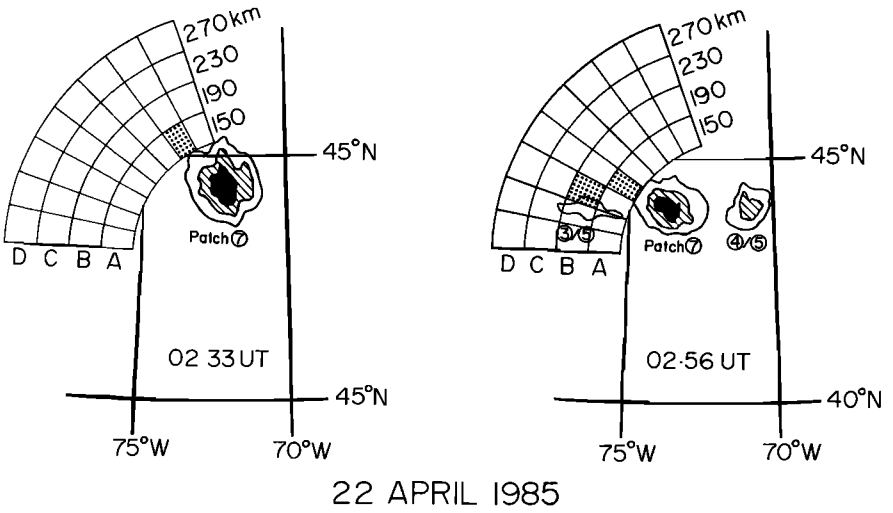

Fig. 8. The radar/optical format described in Figure 7 is used to portray the time history of patch 7 prior to its passage across the radar grid given in Figure 7. At these earlier times, the 150-km-altitude gate showed power enhancements in the "pixel" to the northwest of the 6300-Å patch. The separation of the optical and radar signatures is consistent with a field-aligned process exciting emission at ~ 300 km and plasma enhancements at ~ 150 km (see text).

radar return points. Given that the inclination of geomagnetic field lines near $L = 3$ is ~ 70°, a field-aligned process that produces emission at ~ 300 km and density signatures at 150 km would have a horizontal separation of ~ 60 km, approximately in agreement with the features in Figure 8.

DMSP energetic particle data relevant to the patches are presented in Figure 9. As shown in Figure 5, the DMSP F6 satellite at 1900 MLT crossed the observation region approximately 1 hour 45 min prior to the onset of optical measurements. The ion and electron data in Figure 9*a* show a clear set of boundaries beginning at L=4.5; if optical measurements had been possible at this time, the diffuse aurora produced by these particles would have been beyond the northern limit of the imager's FOV. However, any op-

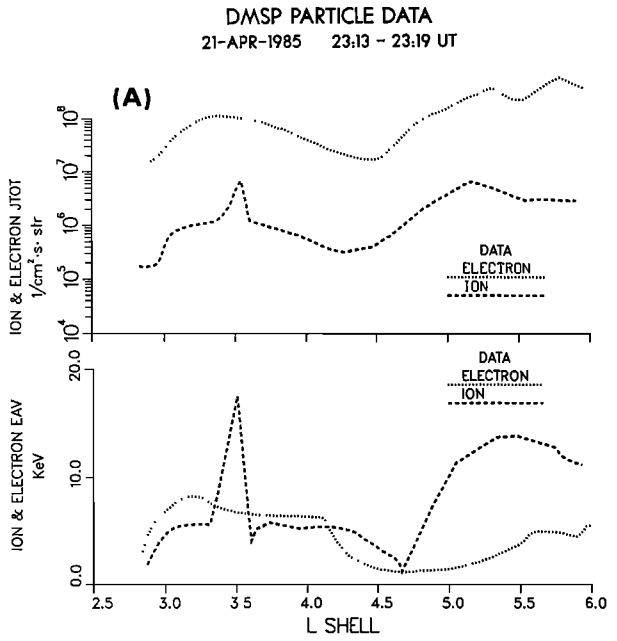

Fig. 9(*a*). DMSP particle data for electron and ion fluxes and average energies from the F6 satellite in an approximately dawn-dusk orbit. The measurements at ~ 2315 UT on April 21, 1985, correspond to ~ 1900 MLT, nearly 2 hours before sky conditions were dark enough to initiate low-light-level imaging observations. The subsatellite track is plotted in Figure 5. Note that the ion precipitation feature at $L = 3.5$ corresponds to the location where patches were observed (and specifically patch 4) at 0100 UT on April 22.

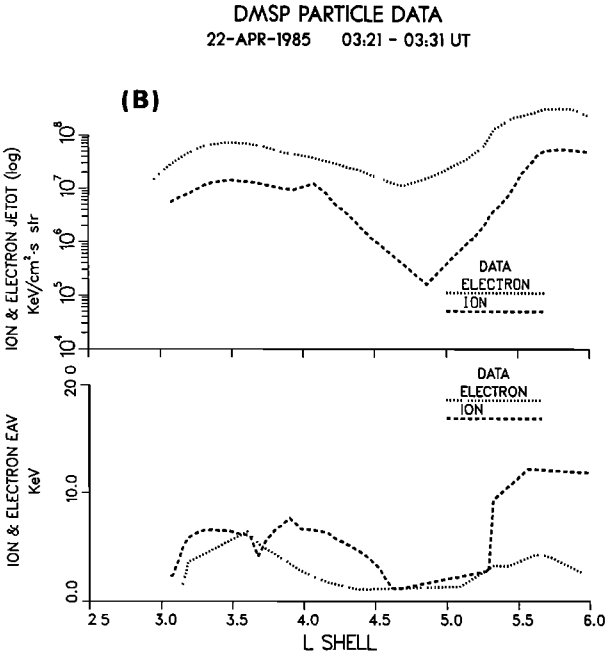

Fig. 9(*b*). DMSP particle data for electron and ion fluxes and average energies from the F7 satellite in an approximately noon-midnight orbit. The measurements at ~ 0325 UT on April 22 correspond to ~ 2200 MLT. The subsatellite track is plotted in Figure 5. Note that the absence of localized ion precipitation features equatorward of the diffuse aurora is consistent with the absence of patches at that time and place. The bright patch 7 does exist well to the west of the satellite track.

tical signatures of the narrow zone of energetic ions at L = 3.5 would have been easily detected. It is intriguing to note that once low-light-level images could be made (at 0100 UT), patch 4 occurred in precisely the area of low-latitude ion precipitation seen 105 min earlier. The lack of diffuse aurora at $L < 4.5$ in the ~ 0100 UT period (Plate 3*a*) is also consistent with a stationary precipitation pattern as portrayed in Figure 9*a*.

Figure 9*b* gives electron and ion data from the DMSP F7 satellite at 2200 MLT that passed close to patch 7 at 0320 UT on April 22 (see Figure 5 and Plate 1*c*). The boundaries at L = 5.2–5.3 place the diffuse aurora beyond the imager's FOV. The absence of a clear low-latitude ion zone is consistent with the lack of optical features beneath the entire subsatellite track. The clear impression we get from Figures 5 and 9 is that the patches are related to ion precipitation effects, with the correlation being more with the ions' energy (> 10 keV) than with their flux levels.

4. DISCUSSION

4.1. *Comparison With Previous Results*

The 6300-Å images of a detached arc, several patches of emission, and ripples in the diffuse aurora offer the first extensive set of ground-based observations of such effects. They extend what had previously been satellite-only observing opportunities to high spatial/temporal measurements that can be conducted in conjunction with other diagnostic techniques (as in the companion paper by *Providakes et al.* [this issue]).

The optical observations described in this paper have as their main goal the specification of the F region signatures of all three phenomena since the ISIS and DMSP imaging systems relate emissions to the 100-km-altitude region. *Wallis et al.* [1979] showed from ISIS particle data that the detached arcs were found at the feet of field lines having a trapped population of electrons with energies 1–10 keV, as well as the usual higher-energy radiation belt particles. They suggested a model in which an injection event near midnight placed particles on drift shells between the plasmapause and the plasma sheet. With a contracted plasmapause, residual plasma sheet electrons drifting about the Earth are precipitated when scattering regions of enhanced cold plasma densities are encountered in the dusk/evening sector. The detached arc is thus the atmospheric image of a magnetospheric cold plasma region. *Wallis et al.* [1979] noted that the ISIS precipitating fluxes peaked near 6 keV (a level harder than observed above the nearby diffuse aurora) and thus were consistent with the observations of *Anger et al.* [1978] that the arc intensities at 6300 Å were much lower than observed at 3914 Å. The image in Plate 1*a* shows the arc brightness to be comparable to the diffuse aurora in 6300 Å, indicating that the precipitation into both regions had to include a soft component as well. This is not necessarily inconsistent with the Wallis et al. and Anger et al. findings since ground-based imaging systems can record fainter 6300-Å structures than was possible with ISIS in 1972–1975. The fact that the TEC enhancement seen within the arc (Figure 6) involves a substantial amount of F region production demonstrates that detached arcs can be an F region phenomenon as well.

Turning to patches, the April 1985 data show that it is difficult to accept the model given by Wallis et al. in which patches arise from the same mechanism as suggested for detached arcs. The plasma measurements given in section 2 show that there is a fundamental difference between detached arcs and patches in that patches have no F region plasma enhancements associated with the optical emission. The DMSP particle data presented in Figure 9 suggest that ions with energies greater than 10 keV may play a more important role than electrons in generating the 6300-Å emission in the patches. As discussed by *Mendillo et al.* [1987], modeling of the November 13, 1983, SAR arc with simultaneously observed N_e and T_e profiles from Millstone Hill failed to yield the observed 6300-Å brightness levels. This suggested that a particle source may be needed to excite Omath (^1D) in F region SAR arcs. As suggested many years ago by *Rees* [1961], ions passing through the F region could leave T_e and N_e unaffected while creating O(^1D). Most of the ions' energy would be deposited below 200 km, which, for the case of patches, would produce the plasma enhancements observed below patches (Figures 7 and 8). The patches may thus represent an elementary form of SAR arcs – resulting from ion fluxes into the ionosphere that might also produce some of the field-aligned current (FAC) signatures recently discovered by *Foster et al.* [1988] from incoherent scatter returns from the trough region.

Finally, the discussion of mechanisms for ripples in the equatorward edge of the diffuse aurora has been presented in detail in the paper by *Providakes et al.* [this issue]. The optical and satellite radio beacon observations presented here document several additional features of undulations in the F region. Plates 1*a* and 2*a* show that the diffuse aurora has an equatorward edge that is, to first order, L shell aligned over the spatial domain accessible to a ground-based all-sky imager. First-order variations in structure occur in the form of undulations (Plates 1*b* and 1*c*) and skewness across L shells (Plates 2*c* and 2*d*). The F region plasma signatures of the diffuse aurora (i.e., the trough's poleward wall) would thus be expected to show similar characteristic features, as discussed by *Providakes et al.* [this issue].

4.2. *Modeling of 6300-Å Airglow*

As described in *Rees and Roble* [1986], there are several production chains for 6300-Å due to auroral (precipitating particle) processes. At mid-latitudes, additional sources arise from normal chemical loss processes (airglow) and thermally excited SAR arcs. While it is beyond the scope of the present paper to compute the total 6300 Å sources from all possible mechanisms, we have conducted simulation studies of the airglow levels generated by the recombination of observed F region profiles. Using the $N_e(h)$ profiles described by *Providakes et al.* [this issue], reaction rates summarized by *Solomon et al.* [1988], and the appropriate Mass Spectrometer and Incoherent Scatter (MSIS) neutral atmosphere [*Hedin*, 1987], we have computed 6300-Å airglow for the regions spanning the trough on April 20 and 21, and for the broad trough minimum region that contained the patches on April 22. The results are presented in Figures 10 and 11 and serve to define the "airglow trough" that results from the well-known F region electron density trough.

On April 20 (Figure 10*a*), a night when clouds prevented optical observations, the model results show airglow levels that are fairly symmetrical across the trough region. The trough center at L_o = 3.5 was flanked by similar profiles at L = 3.1 and 3.9 that yield ~ 55 R. At L = 2.7 (south of the trough), the airglow level of ~ 95 R is actually higher than

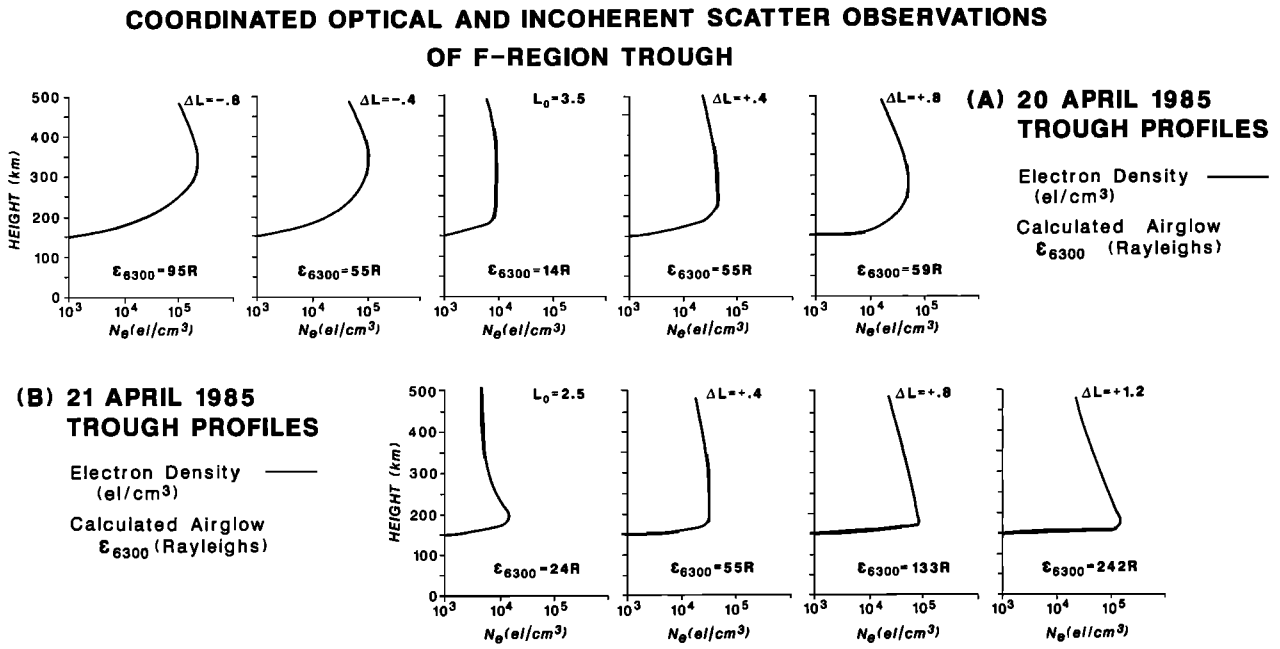

Fig. 10. Observed $N_e(h)$ profiles and calculated airglow for trough region on (*a*) April 20, 1985, and (refit b) April 21, 1985. In both cases, the $N_e(h)$ profiles were taken from *Providakes et al.* [this issue] using their trough coordinate system. The profiles are aligned to show the trough center (L_o = 3.5 on April 20 and L_o = 2.5 on April 21), with profile shapes in ±0.4 L value increments to the north and south.

the recombination airglow in the trough's poleward wall at L = 3.4 (~ 60 R). Of course, the precipitating particles that produce ionization north of the trough also excite the diffuse aurora, and thus we would expect the total 6300-Å levels to be higher in the regions north of the trough. For April 21 (Figure 10*b*), the trough center at L_o = 2.5 placed the equatorward edge beyond the Millstone viewing geometry. The strong poleward wall in F region densities produced airglow levels at L = 3.3 and 3.7 that were 110 R to 220 R above the 6300-Å emission in the trough. The observations near 300 km along the western edge of the FOV in Plate 1*c* show ~ 80 R at L = 2.5, ~ 390 R at L = 3.3 and saturation (> 450 R) at L = 3.7. Thus, for δL = + 0.8 from the trough, the calculated 6300-Å emission increase of 110 R falls well below

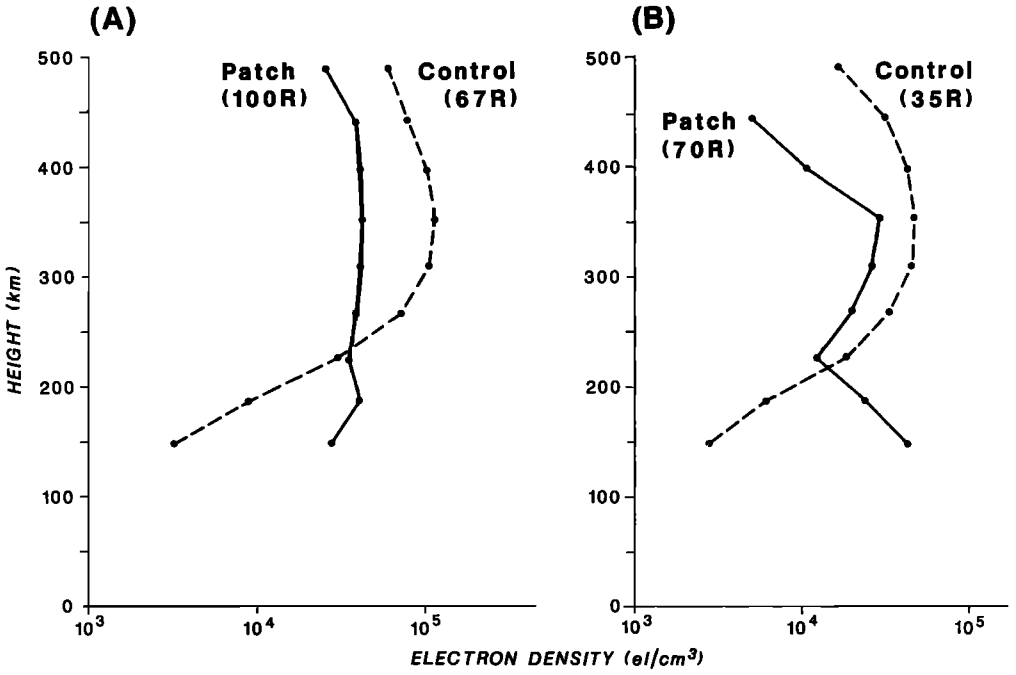

Fig. 11. Observed $N_e(h)$ profiles and calculated airglow for (*a*) patch 2 conditions on April 22, 1985 and (*b*) patch 7 conditions on April 22, 1985 (see text).

the observed 310 R over the same domain, indicating that the particle-induced (diffuse aurora) emission is nearly twice the airglow level produced by the trough's poleward wall. This relationship between the equatorward edge of diffuse aurora and the base of the trough's poleward wall is central to discussions in the companion paper by *Providakes et al.* [this issue Figures 3 and 10] where optical and radar data were compared directly.

For April 22, electron density profiles and their associated 6300-Å airglow are presented in Figure 11*a* for patch 2 and Figure 11*b* for patch 7. These patches are shown in Plates 3*a* and 3*d*, with the Millstone observing grid portrayed in Figure 7. For patch 2, the control curve was obtained by averaging the $N_e(h)$ profiles over azimuths 213°–222°, well to the southwest of the emission features, but still within the trough. The $N_e(h)$ profiles at azimuths 327°–335° were averaged to yield the curve through the 6300-Å patch. For patch 7, a similar set of control and patch $N_e(h)$ profiles were obtained (Figure 11*b*). In both cases, the $N_e(h)$ profiles for the control curves are typical for the equatorward side of the trough minimum ($h_{\max} \sim 350$ km, $N_{\max} \leq 10^5$ el/cm^3). The $N_e(h)$ profiles for the patches have similar shapes above 250 km (with N_{max} lower in the poleward side of the trough minimum). Below 200 km, however, there are large enhancements in the incoherent scatter power returns. Current analysis techniques at Millstone Hill do not handle the complex mix of molecular ions that might occur from precipitation effects into the *E* region. Yet, the spectra from these profiles are not anomalous in the sense of the "false satellite echoes" reported by *Foster et al.* [1988], and thus assuming that O^+ is still the dominant ion should not lead to serious errors in the derived electron density (J. C. Foster, private communication, 1988). In assuming that the power returns below 200 km yield upper limits to the N_e values, the end result is that the derived 6300-Å airglow is still only t~ 35 R higher in a patch than outside it. The observations in Plate 3 show that the total 6300-Å emission inside a patch is typically 300 R brighter than the background in the trough minimum Since the Millstone data for T_e above 300 km (where O^+ spectral analysis is reliable) do not show T_e enhancements typical of SAR arcs [*Rees and Roble*, 1975], we can rule out both airglow and thermal emission mechanisms as significant contributors to the observed signal. With no *F* region density enhancements associated with patches, we also eliminate plasma sheet precipitation typical of diffuse aurora and trough poleward wall locations. This leaves the ion fluxes shown in Figure 9 as a possible source for the patch brightness levels.

Optical signatures of ion fluxes have not been widely discussed or modeled. The early work of *Rees* [1961] pointed to mechanisms for generating 6300 Å from proton fluxes. The DE measurements of *Peterson and Shelley* [1984] and the AE-C observations of *Hoffman et al.* [1985] showed various ion populations above theta aurora and Sun-aligned arcs. Since both of these polar cap features have 6300-Å components, there may be a significant role for ions as a source of optical emissions in the *F* region. A more detailed examination of this issue will be the topic of a separate paper. For the present purposes, we wish to establish that while both ions and electrons contributed to the *F* region signatures of detached arcs and the diffuse aurora, the isolated patches of 6300-Å emission seen within the trough seem more related to ion-induced effects.

Acknowledgments. We are pleased to acknowledge the cooperation of John Foster for facilitating the Millstone measurements and for useful discussions, Michael Kelley for suggesting the experimental campaign and for many valuable comments on the analysis, Eva Basinska-Lewin for assistance with the DMSP particle data, Hann-Bin Chuang for the image processing work, Peter Sultan for analysis of the Millstone patch data, Paul Litis for computational assistance in the 6300-Å airglow simulations, William Lahaise for analysis of the optical data sets and figure preparation, and Kathryn Collins for careful preparation of the manuscript. We are grateful to J. A. Klobuchar at AFGL for providing TEC data from Goose Bay and Sagamore Hill. This work was supported in part by AFGL contract F19628-87-K-0015, ONR contract NOO14-87-K-0158 and NSF grant ATM-87-09487 to Boston Univresity. At Cornell University, work was conducted under NSF grant ATM-85-11811. We also acknowledge the Guest Account at Millstone Hill (supported by NSF ATM-84-19117) that provides for access and use of their incoherent scatter radar data base.

The Editor thanks F. Cruetzberg and A. S. Rodger for their assistance in evaluating this paper.

REFERENCES

Anderson, D. N., Modeling the midlatitude F region ionospheric storm using east-west drift and a meridional wind, *Planet. Space Sci.*, 24, 69, 1976.

Anger, C. D., M. C. Moshupi, D. D. Wallis, J. S. Murphree, L. H. Brace, and G. G. Shepherd, Detached auroral arcs in the trough region, *J. Geophys. Res.*, 83, 2683, 1978.

Baumgardner, J., and S. Karandanis, CCD imaging system uses video graphics controller, *Electronic Imaging*, 3, 28, 1984.

Craven, J. D., L. A. Frank, and K. L. Ackerson, Global observations of a SAR arc, *Geophys. Res. Lett.*, 9, 961, 1982.

Evans, J. V. The causes of storm-time increases of the *F* layer at mid-latitudes, *J. Atmos. Terr. Phys.*, 35, 593, 1973.

Foster, J. C., C. del Pozo, K. Groves, and J.-P. St. Maurice, Radar observations of the onset of current driven instabilities in the topside ionosphere, *Geophys. Res. Lett.*, 15, 160, 1988.

Hedin, A. E., MSIS-86 thermospheric model, *J. Geophys. Res.*, 92, 4649, 1987.

Hoffman, R. A., R. A. Heelis, and J. S. Prasad, A Sun-aligned arc observed by DMSP and AE-C, *J. Geophys. Res.*, 90, 9697, 1985

Kelley, M. C., Intense sheared flow as the origin of large-scale undulations of the edge of the diffuse aurora, *J. Geophys. Res.*, 91, 3225, 1986.

Kozyra, J. U., T. E. Cravens, A. F. Nagy, M. O. Chandler, J. H. Brace, N. C. Maynard, D. W. Slater, B. A. Emery, and S. D. Shawhan, Characteristics of a stable auroral red arc event, *Geophys. Res. Lett.*, 9, 973, 1982.

Lui, A. T. Y., C.-I. Meng, and S. Ismail, Large amplitude undulations on the equatorward boundary of the diffuse aurora, *J. Geophys. Res.*, 87, 2385, 1982.

Mendillo, M., Ionospheric total electron content behavior during geomagnetic storms, *Nature*, 234, 23, 1971.

Mendillo, M., A study of the relationship between geomagnetic storms and ionospheric disturbances, *Planet. Space Sci.*, 21, 349, 1973.

Mendillo, M., H. Hajeb-Hosseinieh, and J. A. Klobuchar, Ionospheric disturbances: Evidence for the contraction of the plasmasphere during severe geomagnetic storms, *Planet. Space Sci.*, 22, 223, 1974.

Mendillo, M., J. Baumgardner, J. Aarons, J. Foster, and J. Klobuchar, Coordinated optical and radio studies of ionospheric disturbances: Initial results from Millstone Hill, *Ann. Geophys. Ser. A*, 5, 543, 1987.

Moshupi, M. C., L. L. Cogger, D. D. Wallis, J. S. Murphree, and C. D. Anger, Auroral patches in the vicinity of the plasmapause, *Geophys. Res. Lett.*, 4, 37, 1977.

Peterson, W. K., and E. G. Shelley, Origin of the plasma in a cross–polar cap auroral feature (theta aurora), *J. Geophys. Res.*, 89, 6729, 1984.

Providakes, J., M. C. Kelley, W. E. Swartz, M. Mendillo, and J. Holt, Radar and optical measurements of ionospheric processes associated with intense subauroral electric fields, *J. Geophys. Res.*, this issue.

Rees, M. H., Excitation of high altitude red auroral arcs, *Planet. Space Sci.*, 8, 59, 1961.

Rees, M. H., and R. G. Roble, Observations and theory of the formation of stable auroral red arcs, *Rev. Geophys.*, 13, 201, 1975.

Rees, M. H., and R. G. Roble, Excitation of $O(^1D)$ atoms in aurorae and emission of the [OI] 6300-A line, *Can. J. Phys.*, 64, 1608, 1986.

Solomon. S., P. B. Hays and V. J. Abreu, The auroral 6300-A emission: Observations and modelling, *J. Geophys. Res.*, 93, 9867, 1988.

Tanaka, T., and K. Hirao, Effects of an electric field on the dynamical behavior of the ionospheres and its application to the storm time disturbance of the *F* layer, *J. Atmos. Terr. Phys.*, 35, 1443, 1973.

Wallis, D. D., J. R. Burrows, M. C. Moshupi, C. D. Anger, and J. S. Murphree, Observations of particles precipitating into detached arcs and patches equatorward of the auroral oval, *J. Geophys. Res.*, 84, 1347, 1979.

J. Baumgardner and M. Mendillo, Center for Space Physics, Boston University, 725 Commonwealth Avenue, Boston, MA 02215.

J. Providakes, School of Electrical Engineering, Cornell University, Ithaca, NY 14583.

(Received August 4, 1988;
revised December 9, 1988;
accepted December 9, 1988.)